Nuclear Instruments and Methods in Physics Research A ▮ (▮▮▮▮) ▮▮▮–▮▮▮

Contents lists available at ScienceDirect

Nuclear Instruments and Methods in Physics Research A

journal homepage: www.elsevier.com/locate/nima

Kochen–Specker theorem studied with neutron interferometer

Yuji Hasegawa *, Katharina Durstberger-Rennhofer, Stephan Sponar, Helmut Rauch

Atominstitut, Technische Universität Wien, Stadionallee 2, A-1020 Wien, Austria

ARTICLE INFO

Keywords:
Neutron interferometer
Entanglement
Kochen–Specker theorem
Contextuality
Degrees of freedom

ABSTRACT

The Kochen–Specker theorem shows the incompatibility of noncontextual hidden variable theories with quantum mechanics. Quantum contextuality is a more general concept than quantum non-locality which is quite well tested in experiments using Bell inequalities. Within neutron interferometry we performed an experimental test of the Kochen–Specker theorem with an inequality, which identifies quantum contextuality, by using spin-path entanglement of single neutrons. Here entanglement is achieved not between different particles, but between degrees of freedom of a single neutron, i.e., between spin and path degree of freedom. Appropriate combinations of the spin analysis and the position of the phase shifter allow an experimental verification of the violation of an inequality derived from the Kochen–Specker theorem. The observed violation $2.291 \pm 0.008 \not\leq 1$ clearly shows that quantum mechanical predictions cannot be reproduced by noncontextual hidden variable theories.

1. Introduction

It was Einstein, Podolsky, and Rosen (EPR) [1] and afterwards Bell [2] who shed light on the non-local properties between subsystems in quantum mechanics. Separately Kochen and Specker [3] analysed sets of measurements of compatible observables and found the impossibility of their consistent coexistence, i.e., quantum indefiniteness of measurement results. In their scenario, quantum contextuality, a more general concept compared to non-locality, leads to striking phenomena predicted by quantum theory.

Bell inequalities [2] are constraints imposed by local hidden-variable theories (LHVTs) on the values of some specific linear combinations of the averages of the results of spacelike separated experiments on distant systems. Reported experimental violations of Bell inequalities, e.g. with photons [4], neutrons [5] or atoms [6], suggest that quantum mechanics (QM) cannot be reproduced by LHVTs.

While violations of Bell's inequalities due to nonlocal characters of QM is impressive, conflict between measurements on a single-system is another marvelous prediction of QM, as is first stated by Kochen–Specker [3]. Quantum mechanical peculiarity is not limited to spacelike separated systems, but found in measurements of a composite non-separated system: it is important to investigate the consequences of hidden-variable theories for (massive) non-spacelike separated quantum systems, such as neutrons.

LHVTs form a subset of a larger class of hidden-variable theories known as noncontextual hidden-variable theories (NCHVTs). In NCHVTs the result of a measurement of an observable is assumed to be predetermined and not affected by a (previous or simultaneous) suitable measurement of any other compatible or co-measurable observable. It turns out that there exists a conflict between the predictions of QM and NCHVTs which is predicted by the KS theorem [3].

Here, we describe experimental demonstration of the violation in line with the KS theorem by using a massive quantum systems, in particular, two degrees of freedom of single neutrons within a neutron interferometer.

2. Kochen–Specker theorem

The Kochen–Specker (KS) theorem states that NCHVTs are incompatible with the predictions of QM (for a review see, e.g., Ref. [7]). The theorem is based on two assumptions: (i) value definiteness: all observables defined for a system, e.g. A and B, have predefined values, e.g. $v(A)$ and $v(B)$ and (ii) noncontextuality: a system possesses a property independently of any measurement context, i.e., independently of how the value is measured. Due to assumption of noncontextuality the relations $v(A+B)=v(A)+v(B)$ and $v(A\cdot B)=v(A)\cdot v(B)$ hold for mutually compatible observables, which have a set of common eigenvectors and thus are measurable together. One can show mathematically that it is impossible to satisfy both relations for arbitrary pairs of compatible operators A and B within QM.

The original proof by Kochen and Specker [3] involves 117 vectors in three dimensions. Peres [8] found a simpler proof with nine observables in four dimensions (two spin-$\frac{1}{2}$ particles) which was later extended by Mermin [7] into a state independent proof (Mermin's square). Mermin [9] also showed that for 10 observables in eight dimensions (three spin-$\frac{1}{2}$ particles, Mermin's pentagram) there exists a connection to the Greenberger–Horne–Zeilinger (GHZ) version [10] of Bell's theorem. Up to now

* Corresponding author.
E-mail address: Hasegawa@ati.ac.at (Y. Hasegawa).

0168-9002/$ - see front matter © 2010 Elsevier B.V. All rights reserved.
doi:10.1016/j.nima.2010.06.234

the simplest proof of the KS theorem was found by Cabello [11] which uses 18 vectors in four dimensions.

We give a short explanation of the proof by Peres and Mermin discussed in Ref. [7]. In four dimensions observables are represented by Pauli matrices of two spin-$\frac{1}{2}$ particles σ_i^1 and σ_j^2 where $i,j=\{x,y,z\}$. The square of each matrix is unity, the eigenvalues are ± 1, in each subspace the standard commutation relations for Pauli matrices are satisfied, and the commutator of matrices from different subspaces is zero $[\sigma_i^1,\sigma_j^2]=0$ for any i,j. Consider the following nine observables A_m arranged in a "magic square":

$$\begin{array}{ccccc} \sigma_x^1 & \sigma_x^2 & \sigma_x^1\cdot\sigma_x^2 & \longrightarrow & +1 \\ \sigma_y^2 & \sigma_y^1 & \sigma_y^1\cdot\sigma_y^2 & \longrightarrow & +1 \\ \sigma_x^1\sigma_y^2 & \sigma_y^1\sigma_x^2 & \sigma_z^1\cdot\sigma_z^2 & \longrightarrow & +1 \\ \downarrow & \downarrow & \downarrow & & \\ +1 & +1 & -1 & & \end{array}$$

In each row and column the observables are mutually commuting and hence compatible. In all rows and also in the first two columns the product of the three observables gives +1 but in the last column we get -1 for the product (due to $\sigma_x^k\sigma_y^k=i\sigma_z^k$ for $k=1,2$). Thus the product of all rows and columns is -1. In NCHVTs we assign to each observable a definite value $v(A_m)$. If we take the product over all rows and columns each value $v(A_m)$ appears twice leading to a total product of +1. This contradicts the QM predictions.

In contrast to Bell's theorem the KS theorem does not use statistical predictions but relies on logical contradictions. However, since perfect correlations on which the proof is based are not obtained in real experiments, it is useful to deduce (statistical) inequalities from the KS theorem for experimental tests. There are several proposals to test KS theorem, inequalities which use the assumptions of contextuality together with additional QM predictions, e.g., [12], inequalities which are solely based on the assumptions of contextuality [13] as well as state-independent inequalities [14]. The first experiments were done with single photons [15] and ions [16] confirming a violation of a state-independent version of the inequality.

3. Theoretical considerations for the experiment

Using inequalities derived from the KS theorem [13] one can study statistical violations of non-contextual assumptions. Exploiting interference effects of matter waves together with entanglement in a single-particle system, neutron interferometric experiments [17] are suitable to exhibit phenomena associated with the KS theorem. At the first stage of experimental tests of quantum contextuality, we performed interferometric experiments demonstrating Kochen–Specker-like phenomena [18]. Further theoretical analysis revealed an advanced scheme based on the Peres–Mermin proof of the KS theorem and an experiment with neutron interferometry was proposed [13] and depicted in Fig. 1. Here, an improved test of the KS theorem with single neutrons is described where the entanglement occurs between two degrees of freedom in a single-particle system [19].

For the proof of the KS theorem, we consider single neutrons prepared in a maximally entangled Bell-like state

$$|\Psi_n^{Bell}\rangle=\frac{1}{\sqrt{2}}(|\downarrow\rangle\otimes|\,\mathrm{I}\,\rangle-|\uparrow\rangle\otimes|\,\mathrm{II}\,\rangle) \tag{1}$$

where $|\uparrow\rangle$ and $|\downarrow\rangle$ denote spin-up and spin-down eigenstates of the neutron, and $|\mathrm{I}\rangle$ and $|\mathrm{II}\rangle$ denote the two beam paths in the neutron interferometer [5]. The proof is based on six observables σ_x^s, σ_x^p, σ_y^s, σ_y^p, $\sigma_x^s\sigma_y^p$ and $\sigma_y^s\sigma_x^p$, where the superscripts s and p indicate the spin and path degree of freedom, respectively,

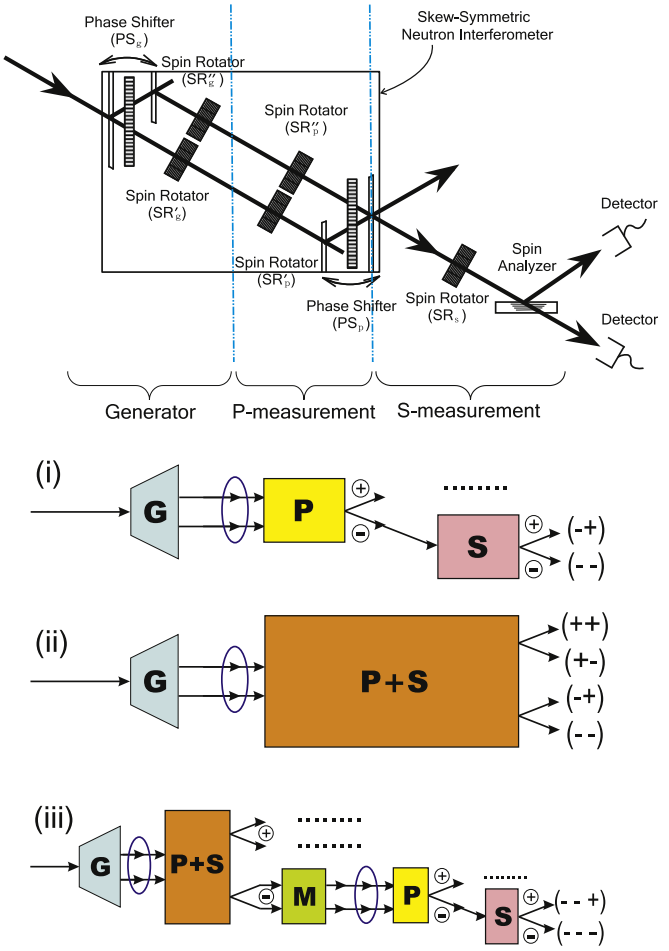

Fig. 1. Above: a proposed experimental setup with a neutron interferometer. The interferometer is set in a way that fulfills two functions: the first half works as a state generator, and the second half works as a path measurement apparatus. In both parts, a phase shifter (PS) and a pair of spin rotators (SR) are inserted. A spin measurement is carried out on the outgoing beam in the forward direction. Below: three diagrams for the different measurement "contexts". (i) For measurements of $\sigma_x^s\cdot\sigma_x^p$ and $\sigma_y^s\cdot\sigma_y^p$: After going through a state generator (G), a state suffers a path measurement (P) followed by a spin measurement (S). Consequently, each outgoing beam gives the results of the two measurements. (ii) For measurements of $\sigma_y^s\sigma_x^p\cdot\sigma_x^s\sigma_y^p$: By tuning one of the spin rotators to a spin-flip operation in the path measurement part, the second half of the interferometer together with a spin analyzer (P+S) can discriminate four Bell states, which assign four outgoing beams to the four possible results of the measurements. (iii) For measurements of $\sigma_y^s\sigma_x^p\cdot\sigma_y^s\cdot\sigma_x^p$ and $\sigma_x^s\sigma_y^p\cdot\sigma_x^s\cdot\sigma_y^p$: After the apparatus P+S, a state mixer (M) eliminates the former information about the result of either observable, and is followed by a path and a spin measurement.

and the following five quantum mechanical predictions for the Bell-like state $|\Psi_n^{Bell}\rangle$:

$$\sigma_x^s\cdot\sigma_x^p|\Psi_n^{Bell}\rangle=-|\Psi_n^{Bell}\rangle \tag{2a}$$

$$\sigma_y^s\cdot\sigma_y^p|\Psi_n^{Bell}\rangle=-|\Psi_n^{Bell}\rangle \tag{2b}$$

$$\sigma_x^s\sigma_y^p\cdot\sigma_x^s\cdot\sigma_y^p|\Psi_n^{Bell}\rangle=+|\Psi_n^{Bell}\rangle \tag{2c}$$

$$\sigma_y^s\sigma_x^p\cdot\sigma_y^s\cdot\sigma_x^p|\Psi_n^{Bell}\rangle=+|\Psi_n^{Bell}\rangle \tag{2d}$$

$$\sigma_x^s\sigma_y^p\cdot\sigma_y^s\sigma_x^p|\Psi_n^{Bell}\rangle=-|\Psi_n^{Bell}\rangle. \tag{2e}$$

The inconsistency arising in any attempt to ascribe the predefined values -1 or +1 to each and every of the six

observables can be easily seen by multiplying Eqs. (2a)–(2e). Since each observable appears twice, the left hand sides give +1 while the product of the right hand sides is -1.

Since experiments cannot show perfect correlations or anti-correlations due to their finite precession, one needs a statistical inequality for experimental testing: the linear combination of the five expectation values with the respective quantum mechanical predictions as linear coefficients. It can be shown that in any NCHVTs

$$-\langle\sigma_x^s\cdot\sigma_x^p\rangle-\langle\sigma_y^s\cdot\sigma_y^p\rangle+\langle\sigma_x^s\sigma_y^p\cdot\sigma_x^s\cdot\sigma_y^p\rangle +\langle\sigma_y^s\sigma_x^p\cdot\sigma_y^s\cdot\sigma_x^p\rangle-\langle\sigma_x^s\sigma_y^p\cdot\sigma_y^s\sigma_x^p\rangle\le 3 \tag{3}$$

in contrast to the prediction of 5 by QM. While Eqs. (2a)–(2b), and (2e) represent state dependent predictions relying on the specific properties of the neutron's Bell-like state $|\Psi_n^{Bell}\rangle$, Eqs. (2c)–(2d) are state-independent predictions which hold in any NCHVTs. In other words, in any NCHVTs, $\langle\sigma_x^s\sigma_y^p\cdot\sigma_x^s\cdot\sigma_y^p\rangle=1$ and $\langle\sigma_y^s\sigma_x^p\cdot\sigma_y^s\cdot\sigma_x^p\rangle=1$. Therefore, any NCHVTs must satisfy not only inequality (3), but also the following inequality in a reduced form:

$$S_{KS}\equiv-\langle\sigma_x^s\cdot\sigma_x^p\rangle-\langle\sigma_y^s\cdot\sigma_y^p\rangle-\langle\sigma_x^s\sigma_y^p\cdot\sigma_y^s\sigma_x^p\rangle\le 1, \tag{4}$$

whereas QM predicts $S_{QM}=3$. A violation of inequality (4) in experiments reveals quantum contextuality.

4. Neutron interferometric experiments

The experiment was carried out at the neutron interferometer instrument S18 at the high-flux reactor of the Institute Laue-Langevin (ILL) in Grenoble, France. The setup of the experiment is depicted in Fig. 2. A monochromatic beam, with mean wavelength $\lambda_0=1.92\,(\Delta\lambda/\lambda_0\sim0.02)$ and $5\times5\,\mathrm{mm}^2$ beam cross-section, is polarized by a bi-refringent magnetic field prism in $\hat{\mathbf{z}}-$direction. Due to the angular separation at the deflection, the interferometer is adjusted so that only the spin-up component fulfills the Bragg condition at the first interferometer plate (beam splitter). Behind the beam splitter the neutron's wave function is found in a coherent superposition of path $|\mathrm{I}\rangle$ and $|\mathrm{II}\rangle$. Together with a radio-frequency (RF) spin-flipper in path $|\mathrm{I}\rangle$, denoted as RF_ω^I, the first half of the interferometer is used for the generation of the maximally entangled Bell-like state, Eq. (1). In this experiment, RF spin-flippers are used for the spin-flips to avoid unwanted contrast reduction due to dephasing effect by the Mu-metal, used in the previous experiment [18]. Apart from the RF flipper in path $|\mathrm{I}\rangle$ our experiment requires a second RF flipper in the interferometer (RF_ω^{II}) and another RF flipper in the O-beam (in the forward direction) operated at half frequency ($\mathrm{RF}_{\omega/2}$).

The first term in inequality (4) requires the measurement of σ_x^s together with σ_x^p. Here, $\mathrm{RF}_{\omega/2}$ in the O-beam is needed for compensating the energy difference due to the spin flip at RF_ω^{I} [20], while the second RF flipper in the interferometer, $\mathrm{RF}_\omega^{\mathrm{II}}$, is turned off. For measuring the path observable, i.e. σ_x^p, the phase shifter is adjusted to $\chi=0$ and π in the path state $|\Psi(\chi)\rangle_p=1/\sqrt{2}(|\mathrm{I}\rangle+e^{i\chi}|\mathrm{II}\rangle)$, which correspond to the projections to $|+x\rangle_p$ and $|-x\rangle_p$, the two eigenstates of σ_x^p, respectively. The spin analysis in the x–y plane is accomplished by the combination of the Larmor accelerator DC coil inducing a Larmor phase $\alpha=0$ and π, a $\pi/2$ DC spin-rotator and an analyzing supermirror. This configuration allows projective measurements along $|+x\rangle_s$ and $|-x\rangle_s$ direction, the two eigenstates of σ_x^s.

The experimental setup for the second term in inequality (4) is identical with the one for the first term, but the measurement of σ_y^s together with σ_y^p is achieved with the settings $\chi=\pi/2,3\pi/2$ and $\alpha=\pi/2,3\pi/2$. Typical intensity oscillations with a contrast of about 67% for the successive measurement of the path and the spin component are shown in Fig. 3 top. The expectation values are experimentally determined from the count rates

$$E(\alpha,\chi)=\frac{N(\alpha,\chi)+N(\alpha+\pi,\chi+\pi)-N(\alpha+\pi,\chi)-N(\alpha,\chi+\pi)}{N(\alpha,\chi)+N(\alpha+\pi,\chi+\pi)+N(\alpha+\pi,\chi)+N(\alpha,\chi+\pi)} \tag{5}$$

where $N(\alpha,\chi)$ denotes the count rate for the joint measurement of spin and path. The required count rates at appropriate settings of α and χ are extracted from least squares fits in Fig. 3 top, indicated by the vertical dashed lines. From these intensities the expectation values were determined as $\langle\sigma_x^s\cdot\sigma_x^p\rangle\equiv E(0,0)=-0.679\pm0.005$ and $\langle\sigma_y^s\cdot\sigma_y^p\rangle\equiv E(\pi/2,\pi/2)=-0.682\pm0.005$. The measured values deviate from the theoretically expected -1 mainly due to the reduced contrast.

The third term in inequality (4) requires the measurement of $\sigma_x^s\sigma_y^p$ together with $\sigma_y^s\sigma_x^p$. Measuring the product of these two observables simultaneously implies the discrimination of the four possible outcomes $(\sigma_x^s\sigma_y^p,\sigma_y^s\sigma_x^p)=\{(+1,+1),(-1,-1),(+1,-1),(-1,+1)\}$, which is equivalent to a complete Bell-state discrimination. The two operators $\sigma_x^s\sigma_y^p$ and $\sigma_y^s\sigma_x^p$ have the four common Bell-like eigenstates

$$|\varphi_\pm\rangle=\tfrac{1}{\sqrt{2}}(|\downarrow\rangle\otimes|\mathrm{I}\rangle\pm i|\uparrow\rangle\otimes|\mathrm{II}\rangle) \tag{6a}$$

$$|\phi_\pm\rangle=\tfrac{1}{\sqrt{2}}(|\uparrow\rangle\otimes|\mathrm{I}\rangle\pm i|\downarrow\rangle\otimes|\mathrm{II}\rangle) \tag{6b}$$

with the corresponding eigenvalue equations

$$\sigma_x^s\sigma_y^p|\varphi_\pm\rangle=\pm|\varphi_\pm\rangle,\sigma_y^s\sigma_x^p|\varphi_\pm\rangle=\mp|\varphi_\pm\rangle \tag{7a}$$

$$\sigma_x^s\sigma_y^p|\phi_\pm\rangle=\pm|\phi_\pm\rangle,\sigma_y^s\sigma_x^p|\phi_\pm\rangle=\pm|\phi_\pm\rangle. \tag{7b}$$

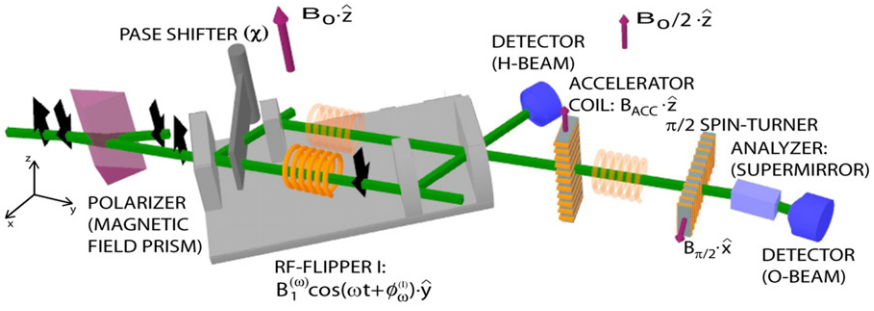

Fig. 2. Experimental setup for studying Kochen–Specker theorem based on the Peres–Mermin proof with neutron interferometer. The RF flipper in the path I (RF_ω^I) generates the Bell-like state $|\Psi_n^{Bell}\rangle$. By turning either the RF flipper in the path II (RF_ω^{II}) or another RF flipper ($RF_{\omega/2}$) on, together with suitable spin analysis, intensity oscillations are obtained in phase shifter χ scans. From the data on the appropriate settings, expectation values of the measurements $\sigma_x^s\cdot\sigma_x^p$,$\sigma_y^s\cdot\sigma_y^p$, and $\sigma_x^s\sigma_y^p\cdot\sigma_y^s\sigma_x^p$ are determined.

Please cite this article as: Y. Hasegawa, et al., Nucl. Instr. and Meth. A (2010), doi:10.1016/j.nima.2010.06.234

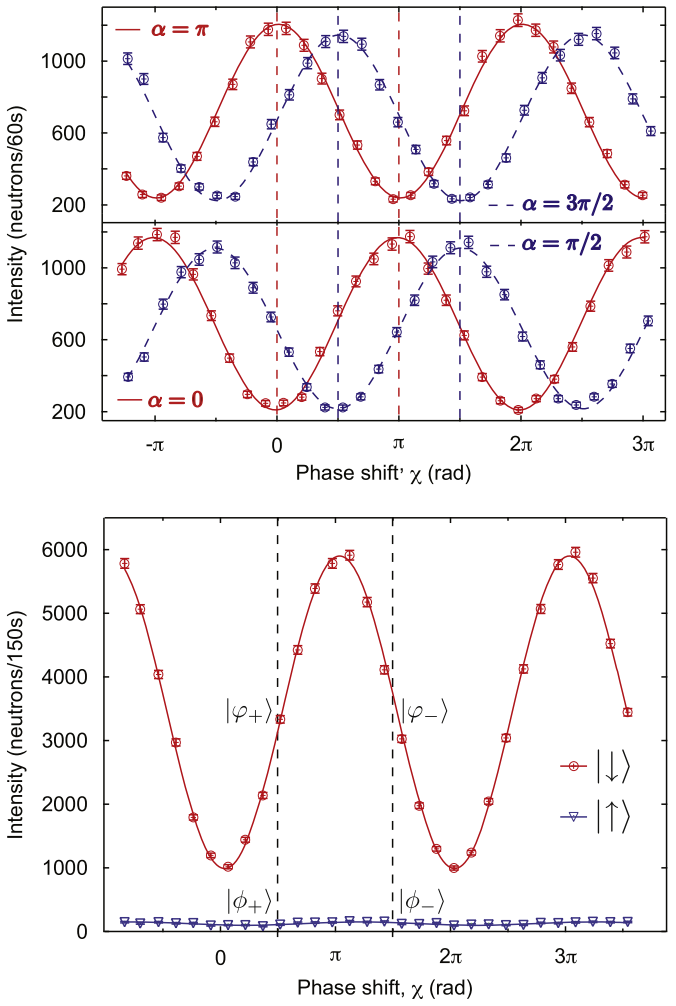

Fig. 3. Typical intensity modulations obtained by varying the phase χ for the path subspace. The spin analysis of $\pm x$- and $\pm y$−directions were involved (top). Another spin-flipper in the interferometer was turned on and the spin analysis of $\pm z$−directions were carried out (bottom).

It follows that the outcome -1 for the product measurement of $\sigma_x^s\sigma_y^p$ and $\sigma_y^s\sigma_x^p$ is obtained for $|\varphi_\pm\rangle$, while the states $|\phi_\pm\rangle$ yield the result +1. In practice, this Bell-state discrimination is accomplished by the second RF flipper in the interferometer, i.e. transforming the state $|\Psi_n^{Bell}\rangle \to 1/\sqrt{2}(|\downarrow\rangle\otimes|\mathrm{I}\rangle - |\downarrow\rangle\otimes|\mathrm{II}\rangle)$. When the DC spin-rotator in the O-beam is adjusted to induce a π−flip, only $|\downarrow\rangle$−spin components reach the detector. Inducing a relative phase χ between the two beam paths in the interferometer allows then for projections to the state $|\varphi(\chi)\rangle = 1/\sqrt{2}(|\downarrow\rangle\otimes|\mathrm{I}\rangle + e^{i\chi}|\uparrow\rangle\otimes|\mathrm{II}\rangle)$. According to the definition of $|\varphi_\pm\rangle$, given in Eq. (6a), phase settings of $\chi = \pm\pi/2$ correspond to the measurement of $|\varphi_\pm\rangle$. The $|\uparrow\rangle$−spin analysis is achieved by switching the DC spin-rotator off, where neutrons in the state $|\phi(\chi)\rangle = 1/\sqrt{2}(|\uparrow\rangle\otimes|\mathrm{I}\rangle + e^{i\chi}|\downarrow\rangle\otimes|\mathrm{II}\rangle)$ can be selected, yielding a $|\phi_\pm\rangle$ measurement for $\chi = \pm\pi/2$. By rotating the phase shifter, clear sinusoidal intensity oscillation and a low-intensity fluctuation were observed, which is depicted in Fig. 3 bottom. The expectation value $\langle\sigma_x^s\sigma_y^p\cdot\sigma_y^s\sigma_x^p\rangle$ is derived using the relation

$$E' = \frac{N'(\phi_+)+N'(\phi_-)-N'(\varphi_+)-N'(\varphi_-)}{N'(\phi_+)+N'(\phi_-)+N'(\varphi_+)+N'(\varphi_-)} \tag{8}$$

where N' denotes the neutron count rate at the desired projections. As done before, least square fits were applied to deduce the count rates at the four projections. From the intensities on the dashed lines in the figure, we obtained the value $\langle\sigma_x^s\sigma_y^p\cdot\sigma_y^s\sigma_x^p\rangle \equiv E' = -0.93\pm0.003$. The observed intensities reflect the quantum mechanical predictions for the measurement of the four Bell-like states given by the expectation values $\langle\Psi|\varphi_\pm\rangle\langle\varphi_\pm|\Psi\rangle = \frac{1}{2}$ and $\langle\Psi|\phi_\pm\rangle\langle\phi_\pm|\Psi\rangle = 0$. The fidelity of the experimental Bell-state discrimination is estimated roughly to 93%.

With the three experimentally derived expectation values we can finally test inequality (4). We obtain

$$S_{\mathrm{exp}} = 2.291\pm0.008 \not\leq 1 \tag{9}$$

which is below the theoretically predicted value of 3 because of imperfect contrasts in the experiment. This value clearly confirms the conflict with NCHVTs.

5. Concluding remarks

Neutron interferometric testing of the KS theorem is described. Entanglement between degrees of freedom of single neutrons is exploited: a Bell-like state comprising spin-path entanglement is generated. The proof is based on the Peres–Mermin criteria. An inequality was derived for the evaluation of the experimental data. Expectation values of three different contexts are determined: the final result, Eq. (9), clearly exhibits the conflict between NCHVTs and QM. We accomplish further studies of quantum contextuality with the use of triply entangled (spin-path-energy entangled) states for single neutrons. In addition, neutron polarimeter experiments are used for similar studies, where tunable multi-energy levels in addition to spin can be manipulated with very high efficiency.

Acknowledgements

We thank G. Badurek, H. Bartosik, A. Cabello, S. Filipp, D. Home, J. Klepp, R. Loidl, and C. Schmitzer. This work has been supported partly by the Austrian Fonds zur Föderung der Wissenschaftlichen Forschung (FWF), no. P21193-N20 and Hertha-Firnberg-Programm T389-N16.

References

[1] A. Einstein, B. Podolsky, N. Rosen, Phys. Rev. 47 (1935) 777.
[2] J.S. Bell, Physics 1 (1964) 195.
[3] S. Kochen, E.P. Specker, J. Math. Mech. 17 (1967) 59.
[4] G. Weihs, T. Jennewein, C. Simon, H. Weinfurter, A. Zeilinger, Phys. Rev. Lett. 81 (1998) 5039.
[5] Y. Hasegawa, R. Loidl, G. Badurek, M. Baron, H. Rauch, Nature (London) 425 (2003) 45.
[6] D.N. Matsukevich, P. Maunz, D.L. Moehring, S. Olmschenk, C. Monroe, Phys. Rev. Lett. 100 (2008) 150404.
[7] N.D. Mermin, Rev. Mod. Phys. 65 (1993) 803.
[8] A. Peres, Phys. Lett. A 151 (1990) 107.
[9] D. Mermin, Phys. Rev. Lett. 65 (1990) 3373.
[10] D.M. Greenberger, M.A. Horne, A. Zeilinger, in: M. Kafatos (Ed.), Bell's Theorem, Quantum Theory, and Conceptions of the Universe, Kluwer Academic, Dordrecht, 1989.
[11] A. Cabello, J.M. Estebaranz, G. García-Alcaine, Phys. Lett. A 212 (1996) 183.
[12] C. Simon, C. Brukner, A. Zeilinger, Phys. Rev. Lett. 86 (2001) 4427.
[13] A. Cabello, S. Filipp, H. Rauch, Y. Hasegawa, Phys. Rev. Lett. 100 (2008) 130404.
[14] A. Cabello, Phys. Rev. Lett. 101 (2008) 210401.
[15] E. Amselem, M. Radmark, M. Bourennane, A. Cabello, Phys. Rev. Lett. 103 (2009) 160405.
[16] G. Kirchmair, F. Zähringer, R. Gerritsma, M. Kleinmann, O. Gühne, A. Cabello, R. Blatt, C.F. Roos, Nature (London) 460 (2009) 494.
[17] H. Rauch, S.A. Werner, Neutron Interferometry, Clarendon Press, Oxford, 2000.
[18] Y. Hasegawa, R. Loidl, G. Badurek, M. Baron, H. Rauch, Phys. Rev. Lett. 97 (2006) 230401.
[19] H. Bartosik, J. Klepp, C. Schmitzer, S. Sponar, A. Cabello, H. Rauch, Y. Hasegawa, Phys. Rev. Lett. 103 (2009) 040403.
[20] S. Sponar, J. Klepp, R. Loidl, S. Filipp, G. Badurek, Y. Hasegawa, H. Rauch, Phys. Rev. A 78 (2008) 061604(R).